ACS APPLIED MATERIALS & INTERFACES

Research Article

www.acsami.org

# One-Step Interface Engineering for All-Inkjet-Printed, All-Organic Components in Transparent, Flexible Transistors and Inverters: Polymer Binding

Jewook Ha,[‡,†] Seungjun Chung,[§,†] Mingyuan Pei,[⊥] Kilwon Cho,[∥] Hoichang Yang,[*,⊥] and Yongtaek Hong[*,‡]

[‡]Department of Electrical and Computer Engineering (ECE), Inter-university Semiconductor Research Center (ISRC), Seoul National University, Seoul 08826, Republic of Korea

[§]Department of Physics and Astronomy, Seoul National University, Seoul 08826, Republic of Korea

[⊥]Department of Applied Organic Materials Engineering, Inha University, Incheon 22212, Republic of Korea

[∥]Department of Chemical Engineering, Pohang University of Science and Technology, Pohang 37673, Republic of Korea

Supporting Information

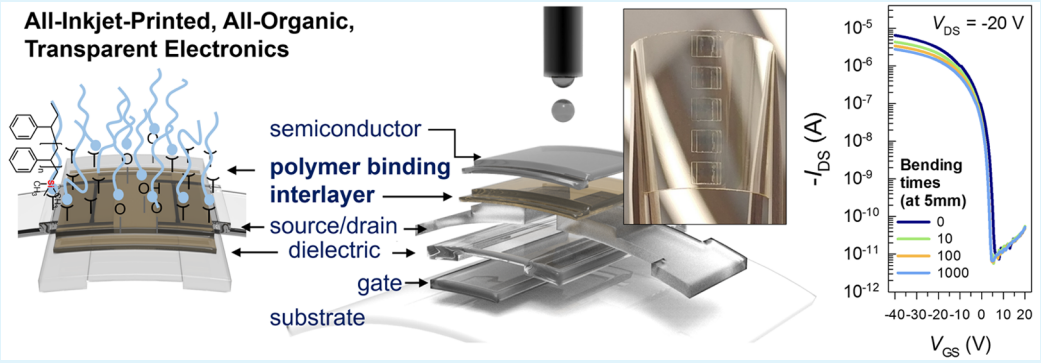


**ABSTRACT:** We report a one-step interface engineering methodology which can be used on both polymer electrodes and gate dielectric for all-inkjet-printed, flexible, transparent organic thin-film transistors (OTFTs) and inverters. Dimethylchlorosilane-terminated polystyrene (PS) was introduced as a surface modifier to cured poly(4-vinylphenol) dielectric and poly(3,4-ethylenedioxythiophene):polystyrenesulfonate (PEDOT:PSS) electrodes without any pretreatment. On the untreated and PS interlayer-treated dielectric and electrode surfaces, 6,13-bis(triisopropylsilylethynyl)pentacene was printed to fabricate OTFTs and inverters. With the benefit of the PS interlayer, the electrical properties of the OTFTs on a flexible plastic substrate were significantly improved, as shown by a field-effect mobility ($\mu_{FET}$) of 0.27 $cm^2 V^{-1} s^{-1}$ and an on/off current ratio ($I_{on}/I_{off}$) of greater than $10^6$. In contrast, the untreated systems showed a low $\mu_{FET}$ of less than 0.02 $cm^2 V^{-1} s^{-1}$ and $I_{on}/I_{off} \sim 10^4$. Additionally, the all-inkjet-printed inverters based on the PS-modified surfaces exhibited a voltage gain of 7.17 $V V^{-1}$. The all-organic-based TFTs and inverters, including deformable and transparent PEDOT:PSS electrodes with a sheet resistance of 160−250 $\Omega\,sq^{-1}$, exhibited a light transmittance of higher than 70% (at wavelength of 550 nm). Specifically, there was no significant degradation in the electrical performance of the interface engineering-assisted system after 1000 bending cycles at a radius of 5 mm.

**KEYWORDS:** *interface engineering, inkjet printing, polymer binding, transparent thin-film transistors, organic thin-film transistors, polymer electrodes*

## 1. INTRODUCTION

Solution-processed transparent thin-film transistors (TFTs) have been studied extensively over the past several years, owing to their use in a variety of cost-effective transparent thin-film electronic applications, such as transparent displays,[1−3] sensors,[4−6] memory devices,[7] photodetectors,[8] and smart contact lenses.[9] In this regard, soluble organic, oxide, and carbon-based materials have gained much attention as potential candidates to fabricate transparent electronic devices.[10−12]

Various solution-processed metal oxide layers are employed for these electronic applications because of their high carrier mobilities and concentrations. However, many obstacles to realizing flexible metal oxide-based TFT applications still exist: high-temperature annealing, the presence of organic impurities,

Received: November 16, 2016
Accepted: February 20, 2017
Published: February 20, 2017





DOI: 10.1021/acsami.6b14702
ACS Appl. Mater. Interfaces 2017, 9, 8819−8829

film rigidity, etc.[2,11,13,14] Flexible carbon nanotubes and graphene have been vigorously utilized in soft electronics applications as complementary carbon-based materials.[12,15,16] However, the uniformity and patterning capability of solution-processed carbon-based layers should be improved to realize practical soft electronics. Recently, solution-processed conducting polymers have been widely evaluated as transparent electrodes in low-temperature, simple, large-area, and low-cost printed electronics.[17−19] A mixture of poly(3,4-ethylenedioxythiophene) and polystyrenesulfonate (PEDOT:PSS) is one of the most promising conducting polymers with high optical transparency, conductivity, and thermal stability.[10,17,20] As a conducting electrode, a PEDOT:PSS layer with a work function of 4.9−5.2 eV can allow a low hole-injection barrier for most of *p*-type organic semiconductors, presenting the highest occupied molecular orbital energy level ranging from −5.00 to −5.30 eV.[21−23] Particularly, PEDOT:PSS electrodes can be easily fabricated using an inkjet-printing method, without any dedicated procedures including photolithography.[17,24,25]

In a bottom-gate and bottom-contact organic TFT (OTFT), it should be considered that the polar moieties of PEDOT:PSS electrodes can cause a high contact resistance ($R_c$) and a short conducting path of organic semiconductors, which together yield severe degradation in the electrical performance.[26,27] A large mismatch in the surface energy ($\gamma$) between the bottom source/drain (S/D) electrode and gate dielectric materials develops an undesired and inhomogeneous semiconducting layer, particularly when a transverse printing between the predefined electrodes on the gate dielectrics is performed. Accordingly, many studies have been focused on matching the surface properties of the bottom electrode and gate dielectric to enhance not only the charge injection from the electrode to the semiconductor layer but also the charge-carrier transport along the $\pi$-overlapped semiconducting domains in OTFTs.[28,29]

Nonpolar self-assembled monolayers (SAMs) or grafted polymer layers may yield organo-compatible dielectric surfaces with fewer charge-trapping sites.[30,31] As one of the most popular treatment methods, the introduction of proper SAMs onto the S/D electrode and dielectric surfaces is well-known to yield optimized surface properties, as well as achieve better ohmic contact and charge transport paths.[32,33] However, low molecular weight ($M_w$) organo-silanes, or -carboxylic acids, -thiols, etc., have been utilized in limited capacities because of the complex processing conditions, originating from these poor environmental stability[34,35] and specific surface chemistry (e.g., organo-thiols for Au[36] and organo-silanes for hydroxyl-rich surfaces[37]). To the best of our knowledge, the one-step interface engineering with a SAM compound, which can simultaneously be introduced to both polymer electrode and dielectric materials, has not been studied yet, while the sequential two- or higher-step processes have been reported elsewhere.[38,39] End-functionalized polymers have been extensively used as reactive modifiers in the surface and interface-related nanoscience.[31,37,40,41] Yang and co-workers have reported that the organo-compatibility of polar oxide or polymer dielectrics was enhanced through grafting of chlorosilane-end-terminated polystyrene (PS) to these surfaces.[31,42] In this case, the surface-grafted chains forming brush- or pancake type layers (4−6 nm) could maintain the excellent solvent resistance without any dewetting or delaminating symptoms, even under direct solvent contact.

Here, we report a simple interface engineering method for organic-based transparent electrode and dielectric materials, which can be simultaneously modified with end-silane-terminated PS without any preliminary treatment. The solvent-durable polymer layer bound to the bottom electrode and gate dielectric surfaces could considerably improve the electrical performance of all-inkjet-printed OTFTs and inverters including PEDOT:PSS, 6,13-bis(triisopropylsilylethynyl) pentacene (TIPS pentacene), and poly(4-vinylphenol) (PVP) as all-organic electrode, semiconductor, and insulator components, respectively, on a flexible plastic substrate. Optimized OTFTs showed a field-effect mobility ($\mu_{FET}$) of 0.27 $cm^2 V^{-1} s^{-1}$, a threshold voltage ($V_{th}$) of 2.42 V, a subthreshold swing (SS) of 1.16 V $dec^{-1}$, and an on/off current ratio ($I_{on}/I_{off}$) of greater than $10^6$, in comparison to the untreated (no interlayer) systems that demonstrated severely degraded values ($\mu_{FET}$ < 0.02 $cm^2 V^{-1} s^{-1}$; $V_{th}$ = 4.41 V; SS = 4.60 V $dec^{-1}$; $I_{on}/I_{off} \sim 10^4$). Also, the polymer interlayer-introduced inverters yielded a high voltage gain ($A_v = \partial V_{out}/\partial V_{in}$) of 7.17 $V V^{-1}$ at supply voltage ($V_{DD}$) of −20 V. The OTFTs and inverters including transparent PEDOT:PSS electrodes with a sheet resistance ($R_S$) of 160−240 $\Omega$ $sq^{-1}$ exhibited a light transmittance ($T_L$) of higher than 70% [at wavelength ($\lambda$) of 550 nm]. Specifically, there was no significant degradation in the electrical performance of the direct interface engineering-assisted system after 1000 bending−relaxation cycles at a bending radius ($R$) of 5 mm.

## 2. EXPERIMENTAL SECTION

**2.1. Materials and Sample Preparation.** Isopropyl alcohol (IPA, Daejung Chemicals & Metals Co.), propylene glycol methyl ether acetate (PGMEA, ≥ 99.5%, Sigma-Aldrich), and toluene (anhydrous, 99.8%, Sigma-Aldrich) were used as solvents without any purification. PEDOT:PSS (E-157, Contech), PVP ($M_w$ = 25 000 g $mol^{-1}$, Sigma-Aldrich), poly(melamine-*co*-formaldehyde) methylated (PMFM, number-average molecular weight ($M_n$) ∼ 432 g $mol^{-1}$, Sigma-Aldrich), PS-Si$(CH_3)_2$Cl ($M_n$ = 7800 g $mol^{-1}$, PDI = 1.06, Polymer Source Inc.), and TIPS pentacene (EM-index Corp.) were purchased and used without any further treatment.

A flexible 200 $\mu$m thick Arylite film (A200HC, Ferrania Corp.) was sequentially ultrasonic-cleaned using IPA and deionized water media. First, as a gate material, the PEDOT:PSS solution was inkjet-printed on the Arylite film while at room temperature, using an inkjet printer (DMP-2831, Dimatix Corp.) with multiple piezo-response nozzles. The resulting gate electrodes were annealed at 130 °C for 30 min. Then, a PVP layer was inkjet-printed on the patterned gate electrode with a solution containing 10 wt % PVP and 2 wt % PMFM dissolved in PGMEA. The layer was thermally cured with a two-step procedure: 100 °C for 20 min and 200 °C for 20 min. On the gate dielectric, PEDOT:PSS S/D electrodes were patterned with the same printing and annealing conditions used for forming the gate electrodes: channel length ($L$) and width ($W$) were 60 $\mu$m and 1050 $\mu$m, respectively. To introduce a polymer interlayer on the bottom S/D electrode and dielectric surfaces, the electrode and channel region were uniformly covered by a dilute PS-Si$(CH_3)_2$Cl solution inkjet-printed through 16 nozzles. After drying, the sample was cured at 100 °C for 1 h to efficiently bind the PS-Si$(CH_3)_2$Cl to these surfaces, and the unbound residues were removed via rinsing with an excess of toluene: the sample was sequentially immersed in toluene for 1 min and dried at 100 °C for 10 min in order to remove residual toluene.

Finally, TIPS pentacene OTFTs and inverters were fabricated on the untreated and polymer-treated bottom S/D electrode and dielectrics. A solution ink of TIPS pentacene dissolved in toluene was inkjet-printed on the bottom surfaces to form the drop spacing (see Figure S1 in the Supporting Information) of 5 $\mu$m and the drop velocity of 5 m $s^{-1}$ with a piezoelectric inkjet head, which contains independently controllable nozzles, at room temperature in ambient air. Then, the coating layer of TIPS pentacene was completely dried at room temperature for 1 h in air. The detailed jetting parameters of each layer inkjet-printed are summarized in Table S1. Additionally, transparent and flexible TIPS pentacene-based inverters were fabricated, including one diode-connected


DOI: 10.1021/acsami.6b14702
ACS Appl. Mater. Interfaces 2017, 9, 8819−8829

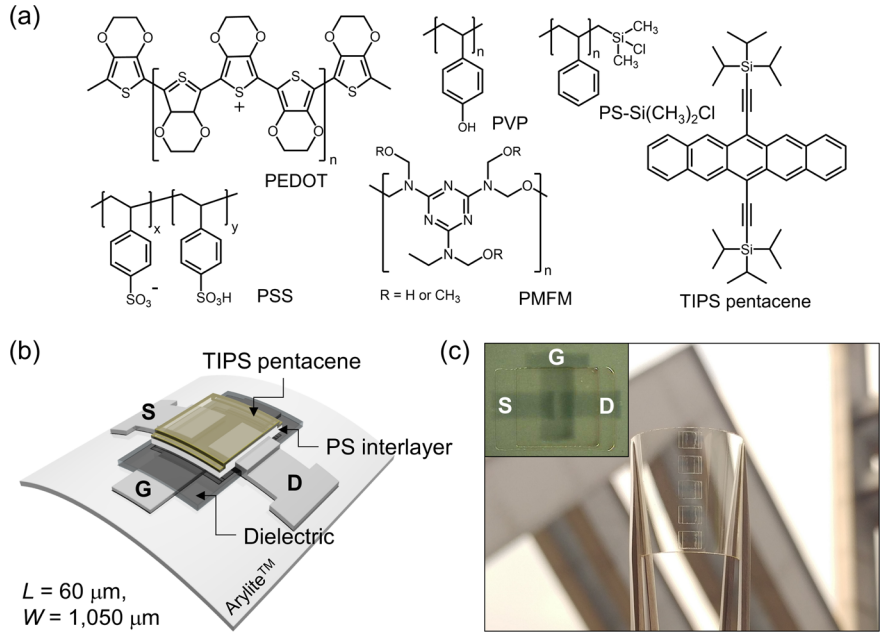


**Figure 1.** (a) Chemical structures of the materials used in this study. (b) Scheme and (c) digital image of all-inkjet-printed TIPS pentacene OTFTs on an Arylite substrate (a microscopic image of the device is also included in the inset).

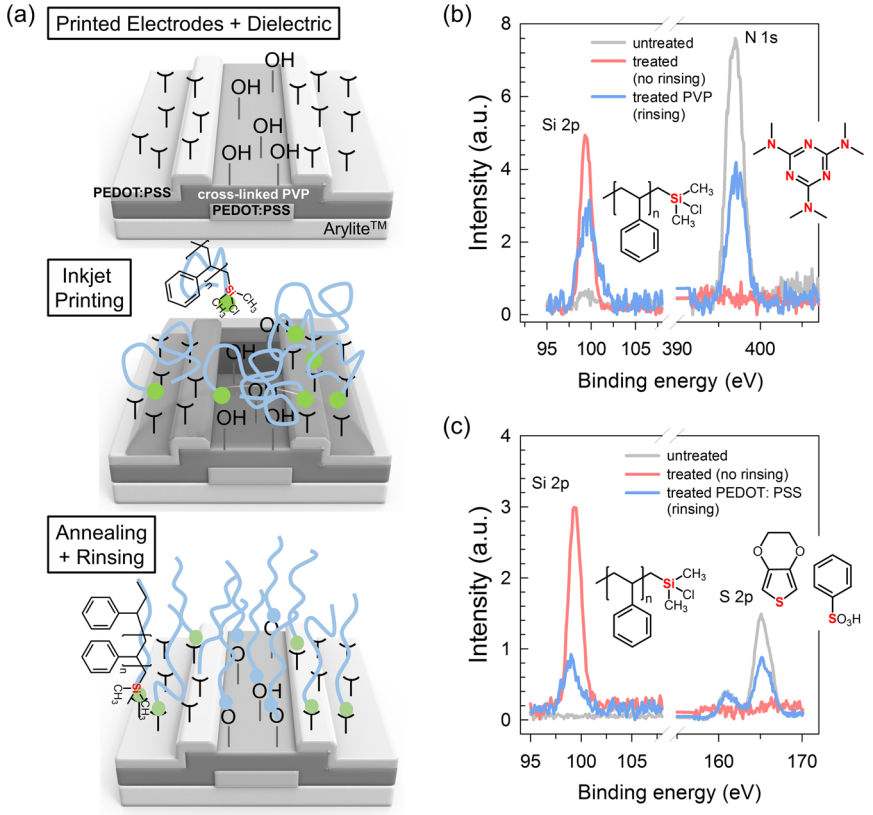


**Figure 2.** (a) Binding scheme of PS-Si$(CH_3)_2$Cl to the predefined PEDOT:PSS and PVP surfaces on gate-patterned Arylite substrate. XPS spectra of untreated and PS-Si$(CH_3)_2$Cl-treated (b) PVP and (c) PEDOT:PSS films on substrates, before and after rinsing with an excess of toluene.

load OTFT ($W/L$ = 440 $\mu$m/320 $\mu$m) and one driver OTFT ($W/L$ = 2050 $\mu$m/80 $\mu$m).

**2.2. Characterization.** The electrical properties of all the OTFTs and inverters were measured using a semiconductor parameter analyzer (4145B, Agilent Technologies) in a dark box. Scanning electron microscopy (SEM) was conducted on TIPS pentacene films inkjet-printed on the S/D electrode and dielectric surfaces using a field emission SEM (FE-SEM, S-4800, Hitachi Corp.). The transmittance measurement was conducted on a bare Arylite film, PEDOT:PSS layers, and all-printed devices on Arylite substrate using a spectrophotometer (DU-70, Beckman). The thicknesses of all printed layers were measured using a surface profiler (Alpha-step 500, Tencor Instruments), and morphologies were measured using an atomic force microscopy instrument (AFM, XE-100, Park Systems Corp.). To determine the surface moieties



DOI: 10.1021/acsami.6b14702
ACS Appl. Mater. Interfaces 2017, 9, 8819−8829

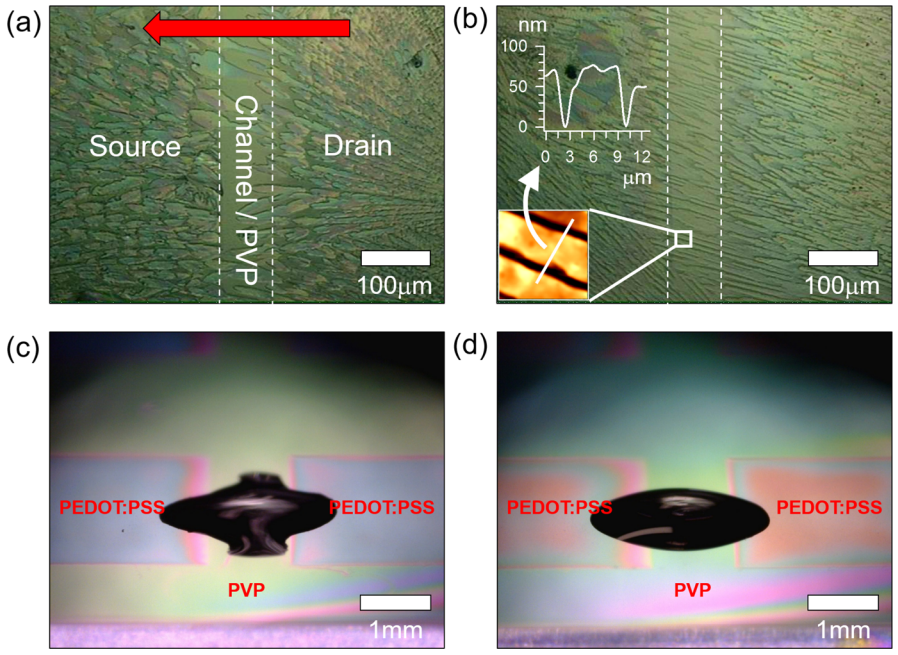


**Figure 3.** OM images of TIPS pentacene films inkjet-printed on the (a) untreated and (b) polymer-treated PEDOT:PSS and PVP surfaces. The red arrow in panel a represents the inkjet-printing direction of the TIPS pentacene ink from the one electrode to the other, and the insets in panel b represent AFM topography and a cross-sectional profile collected from the white-boxed region in the channel area. Wetting characteristics of the TIPS pentacene solutions located on the (c) untreated and (d) polymer-treated PEDOT:PSS and PVP surfaces.

on the electrodes and dielectrics, X-ray photoelectron spectroscopy (XPS, Axis-HSI, Kratos Inc.) was conducted with an Al monochromator anode and a power of 18 mA and 12 kV. Ultraviolet photoelectron spectroscopy (AXIS Ultra DLD, Kratos Inc.) was performed on printed PEDOT:PSS layer with a He−I photon source. Mechanical properties of PEDOT:PSS and silver (Ag, DGP 40LT-15C, ANP Corp.) layers were measured using a nanoindenter (TI 900TriboIndenter, Hysitron Corp.).

## 3. RESULTS AND DISCUSSION

**3.1. Inkjet-Printing of TIPS Pentacene OTFTs.** Figure 1 shows the chemical compounds, scheme, and real image of the all-inkjet-printed, all-organic, transparent TIPS pentacene-based OTFTs on a 200 $\mu$m thick flexible Arylite film. All organic components in the device were sequentially printed on the flexible substrate with the following orders: gate, dielectric, S/D electrode, optionally printed dimethylchlorosilane-terminated PS (PS-Si$(CH_3)_2$Cl) layer, and semiconductor layer. After two-pass printing, a mixture solution of 10 wt % PVP and 2 wt % PMFM as a cross-linker in PGMEA on a PEDOT:PSS gate printed plastic substrate, the printed dielectric was thermally annealed using the curing conditions noted in the Experimental Section.

In previous work, we found that an appropriate ultraviolet−ozone (UV−$O_3$) or plasma treatment on Ag and PVP layers could generate active moieties, which could be coupled with silane-terminated polymers, e.g., PS-Si$(CH_3)_2$Cl.[31] However, it was reported that a UV−$O_3$ exposed PEDOT:PSS layer yielded severe conductivity degradation by the decomposition of PEDOT:PSS, as shown in Figure S2.[43] We proposed a direct treatment of PEDOT:PSS and PVP surfaces with PS-Si$(CH_3)_2$Cl, because sulfonate ($-SO_3^-$) moieties on the PEDOT:PSS electrodes and hydroxyl (−OH) moieties on the PVP gate dielectric can be potential binding sites of the silane-terminated PS (Figure 2a).[44] As an interlayer between the predefined bottom electrode/gate dielectric and top organic semiconductor, a PS-Si$(CH_3)_2$Cl layer ($M_n$ = 7800 g mol$^{-1}$) that was several tens of nanometers thick was inkjet-printed on both the PEDOT:PSS and PVP surfaces using a 0.4 wt % solution dissolved in toluene, and then the printed layer was thermally treated to immobilize the chain ends to both surfaces at 100 °C for 1 h. Finally, the polymer-treated electrode and dielectric surfaces were rinsed with an excess of toluene to remove nonimmobilized residue from these surfaces (Figure 2a). On the basis of our previous works, it was expected that the immobilized polymer layer was a few nanometers thick.[31]

To clarify the proposed interface engineering, XPS was conducted on the PS-Si$(CH_3)_2$Cl-treated PVP and PEDOT:PSS films spun-cast on supporting substrates, before and after toluene rinsing (Figure 2b,c). First, XPS spectra of untreated 500 nm thick PVP and 200 nm thick PEDOT:PSS films did not indicate any binding energy for the Si 2p level. However, the XPS spectra showed intense photoelectron signals at the binding energies of 397.0 and 165.1 eV related to the N 1s and S 2p levels of N and S atoms in PMFM and PSS, respectively (gray lines in Figure 2b,c). Interestingly, the XPS spectra of both the PS-Si$(CH_3)_2$Cl-treated films clearly showed Si 2p peaks at 99.5 eV, irrespective of solvent rinsing. The changes in signal of photoelectrons related to Si 2p, N 1s, and S 2p levels were related to the surface coverage of PS-Si$(CH_3)_2$Cl. Note that most of the collecting photoelectrons were located near the film surface (less than several nanometers).[45] Before solvent rinsing, the XPS spectra of the polymer-treated PVP and PEDOT:PSS samples were mostly acquired from the topmost 20−30 nm thick PS-Si$(CH_3)_2$Cl coating layers, irrespective of the binding types and strength of the polymer to the surfaces. After rinsing, the treated PVP and PEDOT:PSS films with the topmost ultrathin layer of PS-Si$(CH_3)_2$Cl showed the relatively weaker XPS signals of the photoelectrons for N 1s and S 2p than those in the untreated films, maintaining the strong Si 2p peaks. This result can suggest that the PS-Si$(CH_3)_2$Cl chains can sufficiently bind to both PVP and PEDOT:PSS surfaces without any pretreatment.


DOI: 10.1021/acsami.6b14702
ACS Appl. Mater. Interfaces 2017, 9, 8819−8829

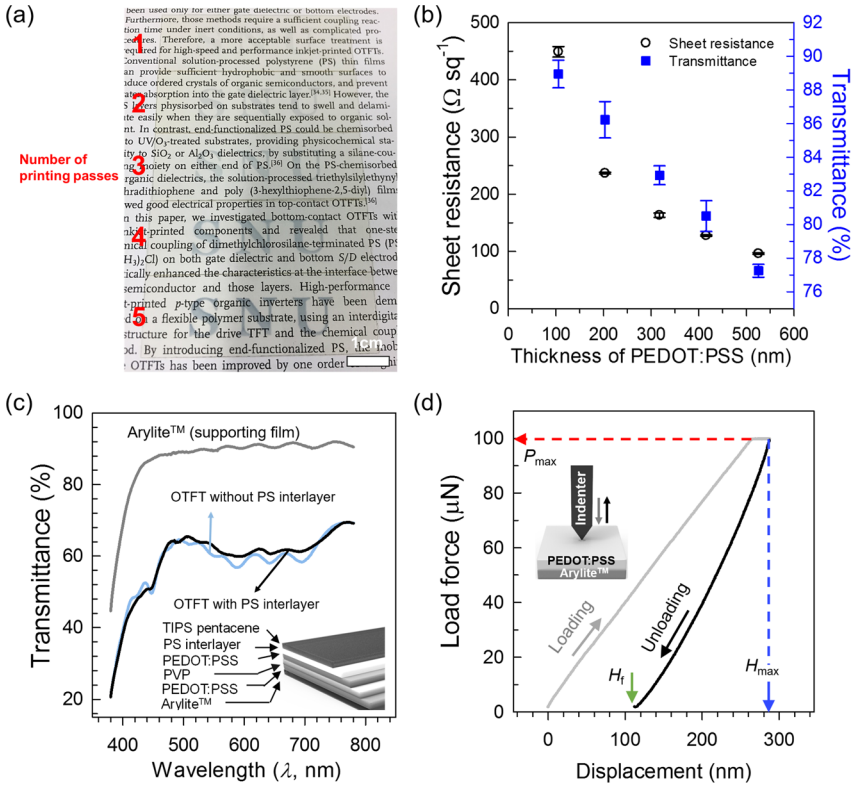


**Figure 4.** (a) "SNU"-letter shaped PEDOT:PSS patterns having different thicknesses inkjet-printed on Arylite films with different number of printing passes from 1 to 5. (b) Optical and electrical characteristics of the PEDOT:PSS electrodes with different thicknesses. The jetting parameters for the PEDOT:PSS layers are summarized in Table S1, specifically, a drop spacing of 25 $\mu$m. (c) $T_L$ variations of an Arylite substrate and fully printed OTFTs. (d) Force−displacement curve of an approximately 350 nm thick PEDOT:PSS layer on the Arylite film during a nanoindenting cycle of loading−unloading (see the inset).

On untreated and PS interlayer-assisted electrode and dielectric surfaces, approximately 70 nm thick TIPS pentacene layers were inkjet-printed and crystallized from the solution in order to complete flexible OTFTs with $L$ of 60 $\mu$m and $W$ of 1050 $\mu$m (Figure 1b). Figure 3a,b shows typical optical microscopy (OM) images of TIPS pentacene layers on the predefined surfaces. The untreated system contained the irregular crystal morphologies of TIPS pentacene, which were clearly observed around the alternated PEDOT:PSS/PVP/PEDOT:PSS (i.e., electrode/dielectric/electrode) surface boundaries (Figure 3a). The result was mainly related to the discernible wettability of the TIPS pentacene solution inkjet-printed onto these heterogeneous surfaces. Among these materials used to generate core components in OTFTs, the difference in $\gamma$ tended to induce a preferred wetting of the TIPS pentacene solution ($\gamma_{\text{TIPS pentacene}}$ = 47.36 mJ m$^{-2}$; $\gamma_{\text{toluene}}$ = 28.52 mJ m$^{-2}$) on the untreated PVP dielectric ($\gamma_{\text{PVP}}$ = 44.07 mJ m$^{-2}$), instead of the hydrophilic PEDOT:PSS electrodes ($\gamma_{\text{PEDOT:PSS}}$ = 67.80 mJ m$^{-2}$) (Figure S3).

On the untreated surfaces, a certain amount of TIPS pentacene solution was quickly dewetted from the hydrophilic PEDOT:PSS side (Figure 3c). During printing, the relatively large volume of the TIPS pentacene solution located on the PVP dielectric side required a longer evaporation time, in comparison to the electrode side. As a result, the TIPS pentacene that was quickly crystallized on the PEDOT:PSS electrodes showed a highly shattered morphology, while on the PVP side, the TIPS pentacene formed layerlike crystallites along the printing direction (arrow in Figure 3a). This kind of wetting behavior on patterned surfaces has also been utilized to develop unique patterns allocated only to predefined regions on a substrate.[24]

In contrast, it was observed that the printed solution on the PS interlayer-assisted electrode and dielectric surfaces was steadily dried, thereby avoiding the coffee-ring effect (Figure 3d). The resulting interlayer-introduced system could modify the electrode and dielectric surfaces to maintain a similar solvent wettability, yielding an enhanced crystal layer of TIPS pentacene along the predefined surfaces (Figure 3b). The PS interlayer effects on the structural development of TIPS pentacene films onto the surfaces are clearly displayed in Figures S4 and S5. Particularly, it was found that a better morphological continuity near the contact region was indicated with the PS-Si$(CH_3)_2$Cl treated system (Figure S5). The solvent wettability-driven crystal morphologies of TIPS pentacene were expected to yield different electrical performances of the resulting OTFTs (will be discussed later).

**3.2. PEDOT:PSS Layers as Transparent Conducting Electrodes.** PEDOT:PSS polymers have been widely utilized as conducting materials for transparent organic electronics applications.[10,24,46] Note that the thicker layer of PEDOT:PSS required to achieve high conductance yields a lower $T_L$. Figure 4a shows digital images of "SNU" letter-shaped PEDOT:PSS patterns inkjet-printed on the Arylite films with a pass number from 1 to 5, which clearly offer different readability.

To investigate the thickness-dependent $R_S$ and $T_L$ of the conducting polymer films, different thick PEDOT:PSS layers were inkjet-printed on a 1 × 1 cm$^2$ area of Arylite films. As expected, the average $R_S$ and $T_L$ (at 550 nm) values of the PEDOT:PSS layers decreased monotonically from 449 to 93 Ω sq$^{-1}$ and from 88.9 to 77.2%, respectively, with an increase in average layer thickness ($h$) ranging from approximately 105 to 525 nm (Figure 4b).


DOI: 10.1021/acsami.6b14702
ACS Appl. Mater. Interfaces 2017, 9, 8819−8829

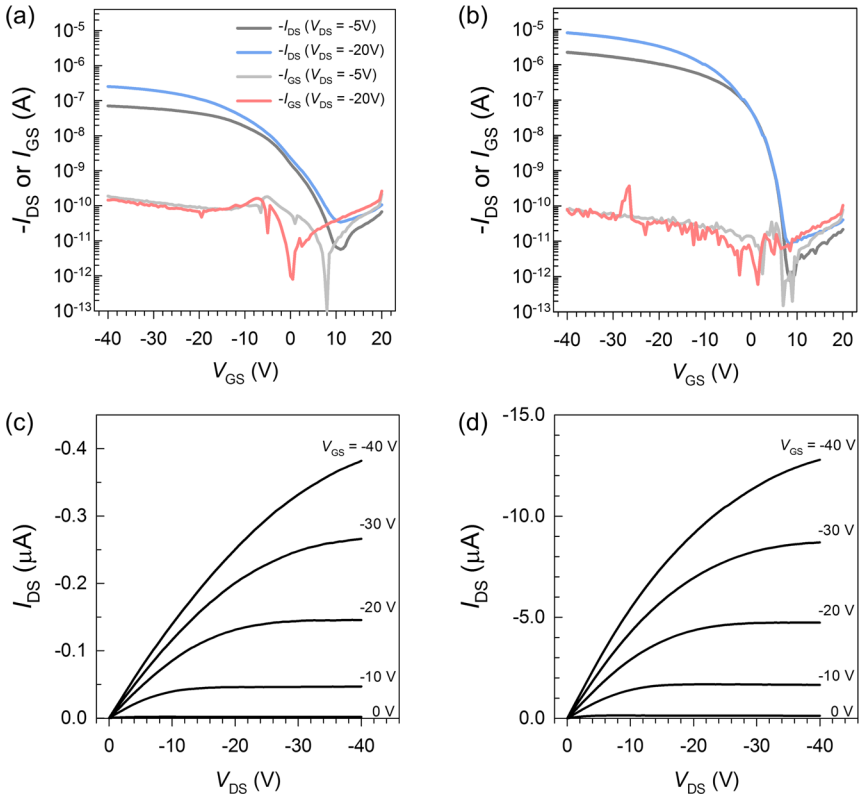


**Figure 5.** (a, b) $I_{DS}$−$V_{GS}$ transfer and (c, d) $I_{DS}$−$V_{DS}$ output curves of TIPS pentacene OTFTs based on the (a, c) untreated and (b, d) PS interlayer-introduced PEDOT:PSS and PVP surfaces.

Although a single-pass printed layer (with $h$ = 105 nm) showed the highest $T_L$ value of 88.9%, its $R_S$ value, 449 Ω sq$^{-1}$, was too high to be used as a conducting electrode. In the all-inkjet-printed OTFTs and inverters, approximately 300 and 200 nm thick PEDOT:PSS layers, as gate and S/D electrodes, were designed to avoid a resistive−capacitive delay and a voltage drop on the electrodes. The average values of $R_S$ for the resulting gate and S/D electrodes were observed to be 163 and 247 Ω sq$^{-1}$, respectively. Additionally, all the printed PEDOT:PSS electrodes showed an average resistivity of 5.0 × 10$^{-3}$ Ω cm, which was higher than those (1−4 × 10$^{-4}$ Ω cm) of highly compact spun-cast PEDOT:PSS layers[47] but comparable to those of inkjet-printed single-walled carbon nanotube (SWCNT) (2.2 × 10$^{-3}$ Ω cm)[12] and solution-processed transparent conductive oxide (e.g., 3.3 × 10$^{-3}$ Ω cm for a gallium-doped zinc oxide[48]) systems reported previously. Particularly, the inkjet-printed PEDOT:PSS layers used in this study showed much better transmittance, surface roughness, and uniformity in comparison to the inkjet-printed SWCNT layer.[12]

Figure 4c shows $T_L$ of a 200 μm thick Arylite film and the fully printed OTFTs on the flexible substrate measured within the visible wavelength ranging from 380 to 780 nm. Note that in order to consider the worst-case in $T_L$, the measured samples were prepared by sequentially printing all organic layers composing the OTFTs over the whole Arylite substrates with the following order: PEDOT:PSS, PVP, PEDOT:PSS, optionally printed PS interlayer, and TIPS pentacene. The samples including the printed OTFTs caused a relatively higher light absorption at λ of 500−720 nm due to the TIPS pentacene layer (Figure S6), in comparison to the bare Arylite film. Interestingly, the presence of the ultrathin PS interlayer (less than 6 nm[31,42]) in the OTFT slightly improved the overall $T_L$ of the device compared to the untreated system including irregular crystal morphology of TIPS pentacene. After the absorption portion is subtracted from the Arylite substrate, the fully printed OTFTs based on the untreated and treated surfaces showed the $T_L$ values of 67.1 and 70.0% (at λ = 550 nm), respectively. These values were comparable to those of previously reported transparent OTFTs with organic or inorganic electrodes.[49,50]

As a flexible electrode, a PEDOT:PSS layer can maintain a sustainable conductance under an external stress, in comparison to the inkjet-printed Ag layer containing percolated nanoparticles. The mechanical properties of PEDOT:PSS layers were evaluated using a nanoindentation method (Figure S7); a well-defined diamond probe (loading resolution < 1 nN) was connected to a vertical transducer and a force gauge. Figure 4d shows the load force−displacement curve of an approximately 350 nm thick PEDOT:PSS layer on the Arylite film during nanoindentation. In general, the elastic and plastic deformations on a film surface simultaneously occur during the loading cycle. In contrast, the recovery of the elastic deformation occurs during the unloading cycle. When the loading−unloading response of the film was investigated, reduced Young's moduli ($E_r$) of the thin films were extracted; a detailed calculation process of $E_r$ from the curve is presented in the Supporting Information. The $E_r$ value of the printed PEDOT:PSS layer was calculated to be 0.61 GPa, much lower than that (47.5 GPa) of an Ag layer inkjet-printed with a similar thickness (Figure S8 and Table S2). Under a stress, the printed PEDOT:PSS electrode is easily deformable, thereby enhancing the bending stability of the resulting OTFTs and inverters (will be also discussed later).

**3.3. Electrical Properties of All-Inkjet-Printed OTFTs and Inverters.** Electrical performance of all-inkjet-printed OTFTs and inverters were characterized in dark conditions.


DOI: 10.1021/acsami.6b14702
ACS Appl. Mater. Interfaces 2017, 9, 8819−8829

Figure 5 shows the drain current−gate voltage ($I_{DS}$−$V_{GS}$) transfer and drain current−drain voltage ($I_{DS}$−$V_{DS}$) output curves of OTFTs including TIPS pentacene layers on the untreated and PS interlayer-assisted S/D and dielectric surfaces. Because of the benefit of the introduced polymer, the maximum interface trap density ($N_{SS}^{max}$) at the semiconductor−dielectric interface in OTFTs decreased up to $5.12 \times 10^{11}$ $cm^{-2}$ $eV^{-1}$, approximately 25.2% of that ($2.03 \times 10^{12}$ $cm^{-2}$ $eV^{-1}$) for the untreated device (details provided in the Supporting Information). Particularly, the presence of the PS interlayer between the PEDOT:PSS and TIPS pentacene surfaces induced a significant decrease in the $R_c$ from 208 to 16.2 kΩ cm, as measured by the transmission line method (TLM) (Figures S9a,b). The outstanding enhancement of a carrier injection property for the polymer-treated system was indicated by the improved linearity in the output curves at low $V_{DS}$ regime (Figure S9c). The result strongly supported that the wettability-matching interface engineering could improve the minimization of the charge trap sites and the better contact and crystal structure of the organic semiconductor. It should be noted that the enhanced charge carrier injection properties after the PS-treatment are attributed to the morphological improvements of the TIPS pentacene semiconductor layer near the contact region, not a change of the work-function values of the PEDOT:PSS electrodes (~5.02 eV).

As expected from the morphology of TIPS pentacene on the untreated electrode and dielectric surfaces (Figure 3a), the resulting OTFT showed a severe degradation in the electrical performance: $\mu_{FET}$ of less than 0.02 $cm^2$ $V^{-1}$ $s^{-1}$, $V_{th}$ of 4.41 V, SS of 4.60 V $dec^{-1}$, and $I_{on}/I_{off}$ of ~$10^4$. In contrast, the PS interlayer-introduced OTFTs showed drastic improvement in the electrical performance: $\mu_{FET}$ = 0.27 $cm^2$ $V^{-1}$ $s^{-1}$, $V_{th}$ = 2.42 V, SS = 1.16 V $dec^{-1}$, and $I_{on}/I_{off}$ > $10^6$. The extracted electrical characteristics are summarized in Table 1. The improved

**Table 1. Typical Electrical Characteristics of TIPS Pentacene OTFTs on the Untreated and PS-Si$(CH_3)_2$Cl-Treated Surfaces**

| OTFTs | $\mu_{FET}$ [$cm^2$ $V^{-1}$ $s^{-1}$] | $V_{th}$ [V] | SS [V $dec^{-1}$] | $I_{on}/I_{off}$ |
|---|---|---|---|---|
| untreated | 0.017 ± 0.010 | 4.41 ± 1.64 | 4.60 ± 1.01 | ~$10^4$ |
| treated | 0.27 ± 0.058 | 2.42 ± 0.48 | 1.16 ± 0.14 | >$10^6$ |

device performance surpassed the previous works related to TIPS pentacene OTFTs with inkjet-printed PEDOT:PSS[26,27] or Ag electrodes.[31] Detailed electrical characteristics of previously reported transparent OTFTs are also summarized in Table S3.

Based on the all-inkjet-printed OTFTs, an inverter including load ($W/L$ = 440 μm/320 μm) and driver ($W/L$ = 2050 μm/80 μm) OTFTs was designed to be operated with a full-swing mode (Figure 6a).[31] Figure 6b,c show typical output voltage ($V_{out}$)−input voltage ($V_{in}$) transfer curves of TIPS pentacene-based inverters on the untreated and treated surfaces; the $A_v$ is also plotted as a function of $V_{in}$ (see the insets). For the untreated inverter, a smooth $V_{out}$−$V_{in}$ inversion tended to shift to the negative direction with increasing $V_{DD}$ (Figure 6b). However, the treated systems showed much higher $A_v$ value of 7.17 V $V^{-1}$ and maintained a $V_{out}$ value close to 0 V in the negative $V_{in}$ region without a shift of the switching voltage ($V_S$) (Figure 6c). These results were attributed to the PS interlayer-driven improvement in $V_{th}$, SS, and $I_{on}/I_{off}$ (Table 1), as well as a distinguishable ratio of $I_{on}$ between the load and driver OTFTs.

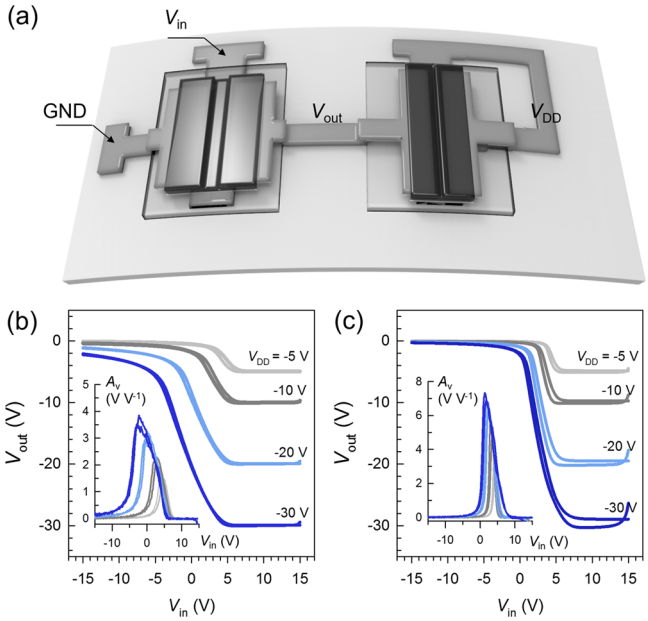


**Figure 6.** (a) Scheme of an inkjet-printed all-organic inverter on a flexible substrate. Voltage-transfer curves of organic inverters on (b) untreated and (c) treated surfaces. The insets represent the corresponding $A_v$−$V_{in}$ curves.

To characterize the bending stability of these flexible devices on the PS interlayer-introduced surfaces, bending tests were conducted on both the OTFTs and inverters (the inset in Figure 7a). During the measurements in a bent state with various $R$ values of 15, 11, 7.5, and 5 mm (Figure 7a) and after 1000 bending−relaxation cycles at $R$ = 5 mm (Figure 7b), no significant changes of electrical characteristics including $\mu_{FET}$, $V_{th}$, SS, and $I_{on}/I_{off}$ were indicated as determined by the $I_{DS}$−$V_{GS}$ transfer curves of the OTFTs. Similarly, the PS interlayer-introduced inverters could maintain the full-swing transition of $V_{in}$ with a slight voltage shift and steady $A_v$ values in a bent state with various $R$ values (Figure 7c) and after 1000 bending−relaxation cycles at $R$ = 5 mm (Figure 7d). The $A_v$−$V_{in}$ curves are also plotted in the insets.

Noise margins, the amount of noise that a logic circuit can tolerate, were also investigated to evaluate a sharp inversion in inverter systems (Figure S10; detailed explanation is presented in the Supporting Information). The high- and low-level noise margins (referred to as $NM_H$ and $NM_L$, respectively) were almost maintained after applying tensile stress during the bending tests. Figures 7e and 7f show variations in $A_v$, $V_S$, $NM_H$, and $NM_L$ of the PS interlayer-introduced inverters, before and after bending. Table 2 summarizes all the electrical characteristics of the untreated and treated inverters. The electrical properties of the untreated OTFTs and inverters and their variations were severely degraded after bending (Figure S11). The PS interlayer-assisted inverters yielded not only intrinsically improved electrical characteristics but also maintained highly consistent values in $A_v$, $V_S$, $NM_H$, $NM_L$, and $V_{out}$ (at $V_{in}$ = −15 V) even after bending. It should be noted that consistent $V_S$, $NM_H$, and $NM_L$ values of the polymer-treated inverters could be attributed to better semiconductor−dielectric interface with lower $N_{SS}^{max}$. These results also clearly indicate that the transparent OTFTs and inverters had excellent flexibility and reliability without significant degradation in the electrical characteristics under tensile stress.


DOI: 10.1021/acsami.6b14702
ACS Appl. Mater. Interfaces 2017, 9, 8819−8829

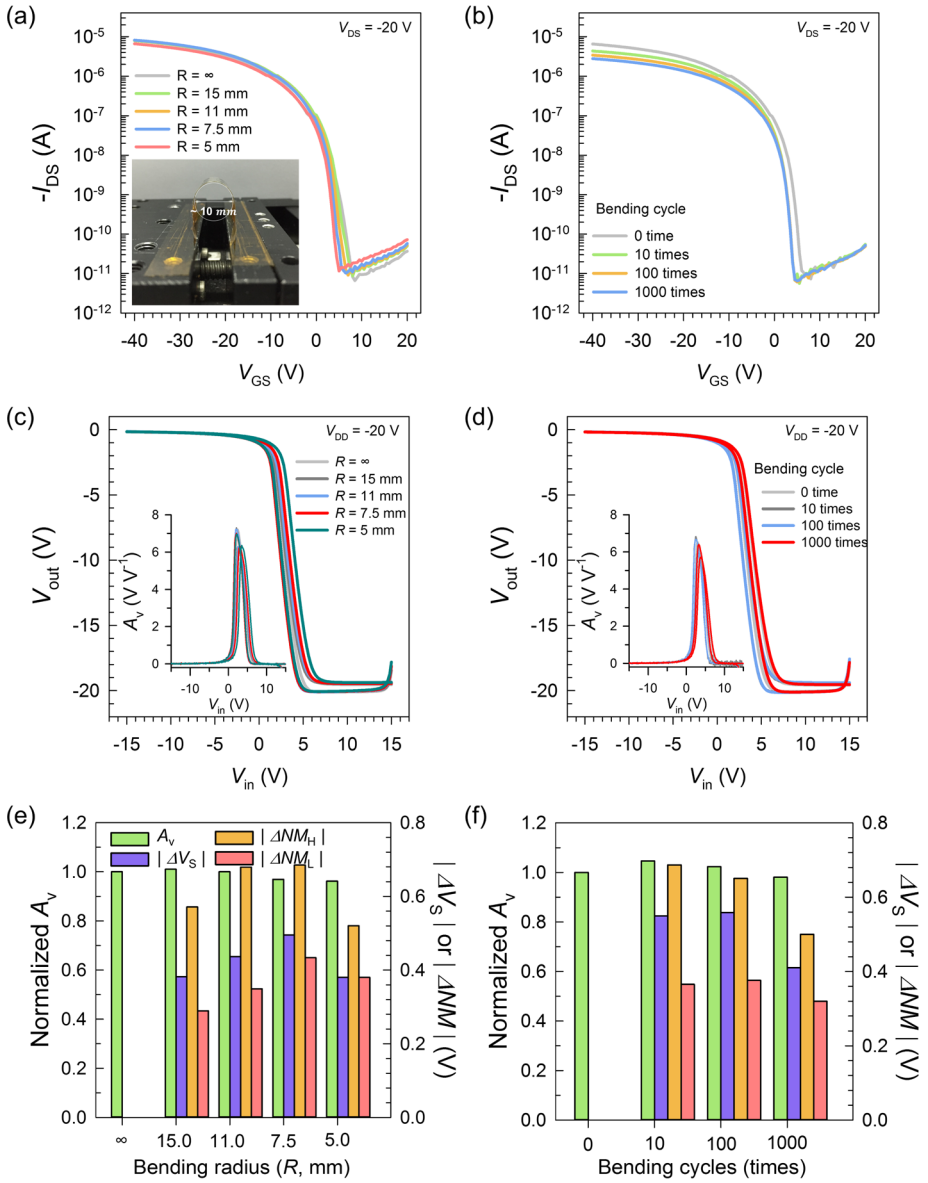


**Figure 7.** (a, b) $I_{DS}$−$V_{GS}$ transfer curves of OTFTs and (c, d) $V_{out}$−$V_{in}$ voltage-transfer curves of organic inverters on the treated surfaces (a, c) in a bent state with various $R$ values and (b, d) after different bending cycles at $R$ = 5 mm. The inset in panel a represents an image of the custom-made bending machine used in this study, and the insets in panels c and d represent the corresponding $A_v - V_{in}$ curves. (e, f) Subsequent relative changes in the electrical characteristics of the inverters.

**Table 2. Variations in the Electrical Performance of the TIPS Pentacene-Based Inverters on Untreated and Polymer-Treated Surfaces, before and after 1000-cycle Bending**

| inverters | bending test | | $A_v$ [V V$^{-1}$] | $\lvert\Delta V_S\rvert$ [V] | $\lvert\Delta NM_H\rvert$ [V] | $\lvert\Delta NM_L\rvert$ [V] | $V_{out}$ [V] (at $V_{in}$ = −15 V) |
|---|---|---|---|---|---|---|---|
| untreated | before | $R = \infty$[a] | 3.03 ± 0.09 | 0 | 0 | 0 | −0.96 ± 0.18 |
| | | $R$ = 5 mm[b] | 2.79 ± 0.06 | 2.50 ± 0.80 | 1.88 ± 0.76 | 2.60 ± 0.79 | −1.16 ± 0.07 |
| | after | $R = \infty$ | 2.62 ± 0.07 | 1.45 ± 0.31 | 1.13 ± 0.28 | 1.56 ± 0.29 | −1.04 ± 0.11 |
| treated | before | $R = \infty$ | 7.17 ± 0.28 | 0 | 0 | 0 | −0.15 ± 0.005 |
| | | $R$ = 5 mm | 6.90 ± 0.16 | 0.38 ± 0.05 | 0.52 ± 0.07 | 0.38 ± 0.06 | −0.15 ± 0.005 |
| | after | $R = \infty$ | 7.03 ± 0.23 | 0.41 ± 0.07 | 0.50 ± 0.08 | 0.32 ± 0.03 | −0.17 ± 0.005 |

[a]No bent state. [b]In a bent state.

## 4. CONCLUSION

We report a simple interface engineering technique for organic-based transparent polymer electrode and dielectric materials, which can be simultaneously modified for binding an end-silane-terminated PS without any preliminary treatment. By using the interface engineering methodology, fully inkjet-printed high-performance transparent OTFTs and inverters were fabricated on flexible Arylite substrates. Considering the trade-off between $T_L$ and $R_S$ of printed PEDOT:PSS electrodes, the number of printing passes for gate and S/D electrodes was optimized.



DOI: 10.1021/acsami.6b14702
ACS Appl. Mater. Interfaces 2017, 9, 8819−8829

The introduction of a polymer interlayer to the electrode and dielectric surfaces could minimize the difference in $\gamma$ between the PEDOT:PSS electrode and PVP dielectric surfaces. The PS interlayer yielded a significant decrease in interface trap density between the gate dielectric and the semiconductor layer and improved the ordering of the TIPS pentacene semiconductor layer. Moreover, the PS interlayer improved carrier injection from the S/D electrodes to the semiconductor layer without degrading $T_L$. The improved OTFTs on the treated surfaces showed a high $\mu_{FET}$ of 0.27 $cm^2 V^{-1} s^{-1}$ (about 15 times higher than that of the untreated OTFTs), $V_{th}$ of 2.42 V, SS of 1.16 V $dec^{-1}$, $I_{on}/I_{off}$ of greater than $10^6$, and $T_L$ of 70.0% (at 550 nm). The organic inverters with the PS interlayer also showed an excellent transition near 0 V, while maintaining $A_v$ of 7.17 $V V^{-1}$ (at $V_{DD} = -20$ V) during a 1000-cycle bending test at $R = 5$ mm. Because all of the layers consisted of soft polymers, much more stable operation under a tensile stress was possible. We believe all-inkjet-printed, all-organic TFTs and inverters on the facilely introduced surface-matching interlayer provide an attractive path toward the realization of high-performance transparent electronics, e.g., transparent display and sensor applications, on a flexible platform with a low-temperature and low-cost process.

## ■ ASSOCIATED CONTENT

### Supporting Information

The Supporting Information is available free of charge on the ACS Publications website at DOI: 10.1021/acsami.6b14702.

Additional sheet resistance, transmittance, wetting behavior, SEM, 2D grazing-incidence X-ray diffraction, and contact resistance data; these analysis methods for the samples (PDF)

## ■ AUTHOR INFORMATION


### Corresponding Authors

*E-mail: hcyang@inha.ac.kr. Phone: +82-32-860-7494.
*E-mail: yongtaek@snu.ac.kr. Phone: +82-2-880-9567.

### ORCID

Kilwon Cho: 0000-0003-0321-3629
Hoichang Yang: 0000-0003-0585-8527


### Author Contributions

†J.H. and S.C. contributed equally to this work.

### Notes

The authors declare no competing financial interest.

## ■ ACKNOWLEDGMENTS

J.H., Y.H., K.C., M.P., and H.Y. appreciate the support from the Center for Advanced Soft-Electronics funded by the Ministry of Science, ICT and Future Planning as Global Frontier Project (2015M3A6A5065309, 2011-0031628, 2012M3A6A5055225). S.C. appreciates the support from the National Creative Research Laboratory program (2012026372) funded by the Korean Ministry of Science, ICT & Future Planning.

## ■ ABBREVIATIONS

AFM, atomic force microscopy
IPA, isopropyl alcohol
$M_n$, number-average molecular weight
$M_w$, molecular weight
OM, optical microscopy
OTFT, organic TFT
PEDOT:PSS, poly(3,4-ethylenedioxythiophene):polystyrenesulfonate
PGMEA, propylene glycol methyl ether acetate
PMFM, poly(melamine-*co*-formaldehyde) methylated
PS, polystyrene
PVP, poly(4-vinylphenol)
S/D, source/drain
SAM, self-assembled monolayer
SEM, scanning electron microscopy
GIXD, grazing-incidence X-ray diffraction
SWCNT, single-walled carbon nanotube
TFT, thin-film transistor
TIPS pentacene, 6,13-bis(triisopropylsilylethynyl)pentacene
TLM, transmission line method
UV−$O_3$, ultraviolet−ozone
XPS, X-ray photoelectron spectroscopy

## ■ REFERENCES


(1) Zhang, J.; Wang, C.; Zhou, C. Rigid/Flexible Transparent Electronics Based on Separated Carbon Nanotube Thin-Film Transistors and Their Application in Display Electronics. *ACS Nano* **2012**, *6*, 7412−7419.

(2) Lee, K.-H.; Kim, S.-M.; Jeong, H.; Pak, Y.; Song, H.; Park, J.; Lim, K.-H.; Kim, J.-H.; Kim, Y. S.; Ko, H. C.; Kwon, I. K.; Jung, G.-Y. All-Solution-Processed Transparent Thin Film Transistor and Its Application to Liquid Crystals Driving. *Adv. Mater.* **2013**, *25*, 3209−3214.

(3) Lee, H. E.; Kim, S.; Ko, J.; Yeom, H.-I.; Byun, C.-W.; Lee, S. H.; Joe, D. J.; Im, T.-H.; Park, S.-H. K.; Lee, K. J. Skin-Like Oxide Thin-Film Transistors for Transparent Displays. *Adv. Funct. Mater.* **2016**, *26*, 6170−6178.

(4) Benfenati, V.; Toffanin, S.; Bonetti, S.; Turatti, G.; Pistone, A.; Chiappalone, M.; Sagnella, A.; Stefani, A.; Generali, G.; Ruani, G.; Saguatti, D.; Zamboni, R.; Muccini, M. A transparent organic transistor structure for bidirectional stimulation and recording of primary neurons. *Nat. Mater.* **2013**, *12*, 672−680.

(5) Sun, Q.; Kim, D. H.; Park, S. S.; Lee, N. Y.; Zhang, Y.; Lee, J. H.; Cho, K.; Cho, J. H. Transparent, low-power pressure sensor matrix based on coplanar-gate graphene transistors. *Adv. Mater.* **2014**, *26*, 4735−4740.

(6) Kim, J.; Lee, M. S.; Jeon, S.; Kim, M.; Kim, S.; Kim, K.; Bien, F.; Hong, S. Y.; Park, J. U. Highly transparent and stretchable field-effect transistor sensors using graphene-nanowire hybrid nanostructures. *Adv. Mater.* **2015**, *27*, 3292−3297.

(7) Shih, C. C.; Lee, W. Y.; Chiu, Y. C.; Hsu, H. W.; Chang, H. C.; Liu, C. L.; Chen, W. C. High Performance Transparent Transistor Memory Devices Using Nano-Floating Gate of Polymer/ZnO Nanocomposites. *Sci. Rep.* **2016**, *6*, 20129.

(8) Liu, X.; Jiang, L.; Zou, X.; Xiao, X.; Guo, S.; Jiang, C.; Liu, X.; Fan, Z.; Hu, W.; Chen, X.; Lu, W.; Hu, W.; Liao, L. Scalable Integration of Indium Zinc Oxide/Photosensitive-Nanowire Composite Thin-Film Transistors for Transparent Multicolor Photodetectors Array. *Adv. Mater.* **2014**, *26*, 2919−2924.

(9) Salvatore, G. A.; Munzenrieder, N.; Kinkeldei, T.; Petti, L.; Zysset, C.; Strebel, I.; Buthe, L.; Troster, G. Wafer-Scale Design of Lightweight and Transparent Electronics that Wraps around Hairs. *Nat. Commun.* **2014**, *5*, 2982.

(10) Vosgueritchian, M.; Lipomi, D. J.; Bao, Z. Highly Conductive and Transparent PEDOT:PSS Films with a Fluorosurfactant for Stretchable and Flexible Transparent Electrodes. *Adv. Funct. Mater.* **2012**, *22*, 421−428.

(11) Jang, J.; Kitsomboonloha, R.; Swisher, S. L.; Park, E. S.; Kang, H.; Subramanian, V. Transparent High-Performance Thin Film Transistors from Solution-Processed $SnO_2/ZrO_2$ Gel-like Precursors. *Adv. Mater.* **2013**, *25*, 1042−1047.

(12) Kim, T.; Song, H.; Ha, J.; Kim, S.; Kim, D.; Chung, S.; Lee, J.; Hong, Y. Inkjet-Printed Stretchable Single-Walled Carbon Nanotube




DOI: 10.1021/acsami.6b14702
*ACS Appl. Mater. Interfaces* 2017, 9, 8819−8829

Electrodes with Excellent Mechanical Properties. *Appl. Phys. Lett.* **2014**, *104*, 113103.
(13) Rim, Y. S.; Jeong, W. H.; Kim, D. L.; Lim, H. S.; Kim, K. M.; Kim, H. J. Simultaneous Modification of Pyrolysis and Densification for Low-Temperature Solution-Processed Flexible Oxide Thin-Film Transistors. *J. Mater. Chem.* **2012**, *22*, 12491−12497.
(14) Chen, Z.; Cotterell, B.; Wang, W.; Guenther, E.; Chua, S.-J. A Mechanical Assessment of Flexible Optoelectronic Devices. *Thin Solid Films* **2001**, *394*, 201−206.
(15) Wu, J.; Becerril, H. A.; Bao, Z.; Liu, Z.; Chen, Y.; Peumans, P. Organic Solar Cells with Solution-Processed Graphene Transparent Electrodes. *Appl. Phys. Lett.* **2008**, *92*, 263302.
(16) Kim, T.; Seong, N.; Ha, J.; Kim, H.; Ha, T.-J.; Hong, Y. The Rapid and Dense Assembly of Solution-Processed Single-Wall Carbon Nanotube Semiconducting Films via an Acid-Based Additive in the Aqueous Dispersion. *J. Mater. Chem. C* **2016**, *4*, 5461−5468.
(17) Lee, M.-W.; Lee, M.-Y.; Choi, J.-C.; Park, J.-S.; Song, C.-K. Fine Patterning of Glycerol-Doped PEDOT:PSS on Hydrophobic PVP Dielectric with Ink Jet for Source and Drain Electrode of OTFTs. *Org. Electron.* **2010**, *11*, 854−859.
(18) Weng, B.; Morrin, A.; Shepherd, R.; Crowley, K.; Killard, A. J.; Innis, P. C.; Wallace, G. G. Wholly Printed Polypyrrole Nanoparticle-Based Biosensors on Flexible Substrate. *J. Mater. Chem. B* **2014**, *2*, 793−799.
(19) Chiolerio, A.; Bocchini, S.; Porro, S. Inkjet Printed Negative Supercapacitors: Synthesis of Polyaniline-Based Inks, Doping Agent Effect, and Advanced Electronic Devices Applications. *Adv. Funct. Mater.* **2014**, *24*, 3375−3383.
(20) Groenendaal, L.; Jonas, F.; Freitag, D.; Pielartzik, H.; Reynolds, J. R. Poly(3,4-ethylenedioxythiophene) and Its Derivatives: Past, Present, and Future. *Adv. Mater.* **2000**, *12*, 481−494.
(21) Schroeder, P. G.; France, C. B.; Park, J. B.; Parkinson, B. A. Energy Level Alignment and Two-Dimensional Structure of Pentacene on Au(111) Surfaces. *J. Appl. Phys.* **2002**, *91*, 3010−3014.
(22) Liu, Y.; Summers, M. A.; Edder, C.; Fréchet, J. M. J.; McGehee, M. D. Using Resonance Energy Transfer to Improve Exciton Harvesting in Organic-Inorganic Hybrid Photovoltaic Cells. *Adv. Mater.* **2005**, *17*, 2960−2964.
(23) Hong, J.-P.; Park, A.-Y.; Lee, S.; Kang, J.; Shin, N.; Yoon, D. Y. Tuning of Ag Work Functions by Self-Assembled Monolayers of Aromatic Thiols for an Efficient Hole Injection for Solution Processed Triisopropylsilylethynyl Pentacene Organic Thin Film Transistors. *Appl. Phys. Lett.* **2008**, *92*, 143311.
(24) Sirringhaus, H.; Kawase, T.; Friend, R. H.; Shimoda, T.; Inbasekaran, M.; Wu, W.; Woo, E. P. High-Resolution Inkjet Printing of All-Polymer Transistor Circuits. *Science* **2000**, *290*, 2123−2126.
(25) Ha, J.; Park, J.; Ha, J.; Kim, D.; Chung, S.; Lee, C.; Hong, Y. Selectively Modulated Inkjet Printing of Highly Conductive and Transparent Foldable Polymer Electrodes for Flexible Polymer Light-Emitting Diode Applications. *Org. Electron.* **2015**, *19*, 147−156.
(26) Basiricò, L.; Cosseddu, P.; Fraboni, B.; Bonfiglio, A. Inkjet Printing of Transparent, Flexible, Organic transistors. *Thin Solid Films* **2011**, *520*, 1291−1294.
(27) Han, J. I.; Kim, Y.-H.; Park, S. K. Enhanced Stability of All Solution-Processed Organic Thin-Film Transistors Using Highly Conductive Modified Polymer Electrodes. *Jpn. J. Appl. Phys.* **2012**, *51*, 091602.
(28) Gundlach, D. J.; Royer, J. E.; Park, S. K.; Subramanian, S.; Jurchescu, O. D.; Hamadani, B. H.; Moad, A. J.; Kline, R. J.; Teague, L. C.; Kirillov, O.; Richter, C. A.; Kushmerick, J. G.; Richter, L. J.; Parkin, S. R.; Jackson, T. N.; Anthony, J. E. Contact-Induced Crystallinity for High-Performance Soluble Acene-Based Transistors and Circuits. *Nat. Mater.* **2008**, *7*, 216−221.
(29) Asadi, K.; Wu, Y.; Gholamrezaie, F.; Rudolf, P.; Blom, P. W. M. Single-Layer Pentacene Field-Effect Transistors Using Electrodes Modified With Self-Assembled Monolayers. *Adv. Mater.* **2009**, *21*, 4109−4114.
(30) Chua, L.-L.; Zaumseil, J.; Chang, J.-F.; Ou, E. C.-W.; Ho, P. K.-H.; Sirringhaus, H.; Friend, R. H. General Observation of n-Type Field-Effect Behaviour in Organic Semiconductors. *Nature* **2005**, *434*, 194−199.
(31) Chung, S.; Jang, M.; Ji, S.-B.; Im, H.; Seong, N.; Ha, J.; Kwon, S.-K.; Kim, Y.-H.; Yang, H.; Hong, Y. Flexible High-Performance All-Inkjet-Printed Inverters: Organo-Compatible and Stable Interface Engineering. *Adv. Mater.* **2013**, *25*, 4773−4777.
(32) Fukuda, K.; Takeda, Y.; Mizukami, M.; Kumaki, D.; Tokito, S. Fully Solution-Processed Flexible Organic Thin Film Transistor Arrays with High Mobility and Exceptional Uniformity. *Sci. Rep.* **2014**, *4*, 3947.
(33) Kitamura, M.; Kuzumoto, Y.; Aomori, S.; Kamura, M.; Na, J. H.; Arakawa, Y. Threshold Voltage Control of Bottom-Contact n-Channel Organic Thin-Film Transistors Using Modified Drain/Source Electrodes. *Appl. Phys. Lett.* **2009**, *94*, 083310.
(34) Lee, H. S.; Kim, D. H.; Cho, J. H.; Hwang, M.; Jang, Y.; Cho, K. Effect of the Phase States of Self-Assembled Monolayers on Pentacene Growth and Thin-Film Transistor Characteristics. *J. Am. Chem. Soc.* **2008**, *130*, 10556−10564.
(35) Virkar, A.; Mannsfeld, S.; Oh, J. H.; Toney, M. F.; Tan, Y. H.; Liu, G.; Scott, J. C.; Miller, R.; Bao, Z. The Role of OTS Density on Pentacene and $C_{60}$ Nucleation, Thin Film Growth, and Transistor Performance. *Adv. Funct. Mater.* **2009**, *19*, 1962−1970.
(36) Lin, W. C.; Lee, S. H.; Karakachian, M.; Yu, B. Y.; Chen, Y. Y.; Lin, Y. C.; Kuo, C. H.; Shyue, J. J. Tuning the Surface Potential of Gold Substrates Arbitrarily with Self-Assembled Monolayers with Mixed Functional Groups. *Phys. Chem. Chem. Phys.* **2009**, *11*, 6199−6204.
(37) Park, S. H.; Lee, H. S.; Kim, J.-D.; Breiby, D. W.; Kim, E.; Park, Y. D.; Ryu, D. Y.; Lee, D. R.; Cho, J. H. A Polymer Brush Organic Interlayer Improves the Overlying Pentacene Nanostructure and Organic Field-Effect Transistor Performance. *J. Mater. Chem.* **2011**, *21*, 15580−15586.
(38) Sonar, P.; Singh, S. P.; Li, Y.; Ooi, Z.-E.; Ha, T.-j.; Wong, I.; Soh, M. S.; Dodabalapur, A. High Mobility Organic Thin Film Transistor and Efficient Photovoltaic Devices Using Versatile Donor−Acceptor Polymer Semiconductor by Molecular Design. *Energy Environ. Sci.* **2011**, *4*, 2288−2296.
(39) Xie, Y.; Cai, S.; Shi, Q.; Ouyang, S.; Lee, W.-Y.; Bao, Z.; Matthews, J. R.; Bellman, R. A.; He, M.; Fong, H. H. High Performance Organic Thin Film Transistors Using Chemically Modified Bottom Contacts and Dielectric Surfaces. *Org. Electron.* **2014**, *15*, 2073−2078.
(40) Li, L.; Hu, W.; Chi, L.; Fuchs, H. Polymer Brush and Inorganic Oxide Hybrid Nanodielectrics for High Performance Organic Transistors. *J. Phys. Chem. B* **2010**, *114*, 5315−5319.
(41) Jang, M.; Park, J. H.; Im, S.; Kim, S. H.; Yang, H. Critical Factors to Achieve Low Voltage- and Capacitance-based Organic Field-Effect Transistors. *Adv. Mater.* **2014**, *26*, 288−292.
(42) Lee, S.; Jang, M.; Yang, H. Optimized Grafting Density of End-Functionalized Polymers to Polar Dielectric Surfaces for Solution-Processed Organic Field-Effect Transistors. *ACS Appl. Mater. Interfaces* **2014**, *6*, 20444−20451.
(43) Nagata, T.; Oh, S.; Chikyow, T.; Wakayama, Y. Effect of UV−Ozone Treatment on Electrical Properties of PEDOT:PSS Film. *Org. Electron.* **2011**, *12*, 279−284.
(44) Lee, J. Y.; Lee, S. T. Laser-Induced Thermal Imaging of Polymer Light-Emitting Materials on Poly(3,4-ethylenedioxythiophene): Silane Hole-Transport Layer. *Adv. Mater.* **2004**, *16*, 51−54.
(45) Livesey, A. K.; Smith, G. C. The Determination of Depth Profiles from Angle-Dependent XPS Using Maximum Entropy Data Analysis. *J. Electron Spectrosc. Relat. Phenom.* **1994**, *67*, 439−461.
(46) Kim, Y. H.; Sachse, C.; Machala, M. L.; May, C.; Müller-Meskamp, L.; Leo, K. Highly Conductive PEDOT:PSS Electrode with Optimized Solvent and Thermal Post-Treatment for ITO-Free Organic Solar Cells. *Adv. Funct. Mater.* **2011**, *21*, 1076−1081.
(47) Cook, J. H.; Al-Attar, H. A.; Monkman, A. P. Effect of PEDOT−PSS Resistivity and Work Function on PLED Performance. *Org. Electron.* **2014**, *15*, 245−250.
(48) Nayak, P. K.; Yang, J.; Kim, J.; Chung, S.; Jeong, J.; Lee, C.; Hong, Y. Spin-Coated Ga-Doped ZnO Transparent Conducting Thin Films for Organic Light-Emitting Diodes. *J. Phys. D: Appl. Phys.* **2009**, *42*, 035102.


DOI: 10.1021/acsami.6b14702
*ACS Appl. Mater. Interfaces* 2017, 9, 8819−8829

(49) Moon, H.; Cho, H.; Kim, M.; Takimiya, K.; Yoo, S. Towards Colorless Transparent Organic Transistors: Potential of Benzothieno-[3,2-*b*]benzothiophene-Based Wide-Gap Semiconductors. *Adv. Mater.* **2014**, *26*, 3105−3110.
(50) Trung, T. Q.; Tien, N. T.; Seol, Y. G.; Lee, N.-E. Transparent and Flexible Organic Field-Effect Transistor for Multi-Modal Sensing. *Org. Electron.* **2012**, *13*, 533−540.



DOI: 10.1021/acsami.6b14702
*ACS Appl. Mater. Interfaces* 2017, 9, 8819−8829